Rare Metal Materials and Engineering
Volume 51, Issue 12, December 2022
Available online at www.rmme.ac.cn

Science Press

Cite this article as: Chu Linhua, Zhang Shuyan, Yuan Gaihuan, et al. Effect of Trace Nickel Addition on Microstructure, Corrosion Resistance and Hydrogen Absorption of Zr-4 Alloy[J]. Rare Metal Materials and Engineering, 2022, 51(12): 4488-4495.

ARTICLE

Effect of Trace Nickel Addition on Microstructure, Corrosion Resistance and Hydrogen Absorption of Zr-4 Alloy

Chu Linhua[1], Zhang Shuyan[1], Yuan Gaihuan[2], Wu Guiyi[1]

[1] Centre of Excellence for Advanced Materials, Dongguan 523808, China; [2] State Nuclear BaoTi Zirconium Industry Company, Baoji 721013, China

Abstract: Nickel as a trace element was added into zirconium alloy (Zr-4) and then alloy sheet samples were prepared. The microstructure, corrosion property, and hydrogen content of the Zr-4 alloy were studied. Results show that the steam corrosion resistance at 400 °C can be greatly improved by adding nickel from 0.001wt% (the content in the sponge zirconium) to 0.005wt%, and there is no obvious effect on hydrogen absorption property. Trace nickel addition increases the content of the second phase particles in the form of $Zr(Fe, Ni)_2$ obviously, and promotes the aggregation of silicon around second phase particles, which can prevent or delay the oxidation of fine particles. In addition, zirconium tubes (Φ63.5 mm×10.92 mm) with the same alloy component also exhibit excellent nodular corrosion resistance and uniform corrosion resistance.

Key words: nickel; Zr-4; microstructure; corrosion resistance; hydrogen absorption; aggregation; oxidation

Zirconium alloys (Zircaloy-2 and Zircaloy-4) have been used as structural materials in boiling-water reactors (BWRs) and pressurized-water reactors (PWRs) for many years due to their excellent nuclear properties, especially the anti-corrosion and mechanical properties in reactors[1-4]. Alloying composition[5-8], material processing[9-12], surface states[13,14], and corrosion environment[15] are important factors determining the anti-corrosion and hydrogen absorption properties. Among these factors, alloying composition is the most important intrinsic factor for the corrosion properties.

Many studies have shown that the corrosion properties of zirconium alloys are closely related to the quantity, size, and distribution of second phase particles[16-19]. In order to improve the corrosion resistance, alloying elements are added to zirconium alloys, such as Fe, Cr, and Ni. Because the solubility of alloying elements are limited, second phase particles are usually formed and dispersed along grain boundaries which are closely related to corrosion properties. For example, $Zr(Fe, Cr)_2$ and $Zr_2(Fe, Ni)$ are the precipitates inside zirconium alloys[20]. The Zr-2 alloy (Fe: 0.07wt% ~ 0.20wt%, Cr: 0.05wt%~0.15wt%, Ni: 0.03wt%~0.18wt%, Fe+Cr+Ni: 0.18wt% ~0.38wt%) was developed for BWRs. Although nickel addition can improve the corrosion resistance, it makes hydrogen absorption properties worse[21]. Once the hydrogen content in Zr-2 alloy goes beyond its solubility, extra hydrogen will precipitate in the form of Zr-H_x particles, which make the zirconium alloy brittle[22]. In order to overcome this problem, Zr-4 (Fe: 0.18wt% ~0.24wt% , Cr: 0.09wt%~0.13wt%, Ni ≤0.007wt%) was developed for PWRs and hydrogen absorption is lowered [23].

The effects of Ni content on the corrosion and hydrogen absorption properties of Zr-Sn alloys have been extensively studied[24-27]. However, there is a gap in the upper bound of Ni content between sponge zirconium and Zr-4. In this work, the effect of Ni content within this gap range was investigated with the zirconium sheet samples. Since zirconium tubes were used as cladding material in the reactors, the zirconium alloy tubes were also fabricated.

1 Experiment

1.1 Sheet sample preparation

Firstly, 25 kg of button ingots were forged with three melting cycles for sheet samples. The ingots with about 160 mm in diameter were supposed to be chemically

Received date: February 26, 2022
Foundation item: Guangdong Innovative and Entrepreneurial Research Team Program (2016ZT06G025)
Corresponding author: Chu Linhua, Ph. D., Senior Engineer, Centre of Excellence for Advanced Materials, Dongguan 523808, P. R. China, Tel: 0086-769-23079125, E-mail: chulinhuascu@163.com

homogeneous. Since low carbon content and high silicon content benefit the corrosion properties of Zr-4 alloy[28], the carbon content was set in the range of 0.002wt%~0.005wt%, and the silicon content was in the range of 0.008wt% ~ 0.012wt%. In order to investigate the effect of nickel content on the corrosion properties of Zr-4 alloy, three categories of Zr-4 samples were fabricated and their nickel contents were: <0.002wt%, 0.002wt% ~0.0040wt%, and 0.004wt% ~ 0.006wt%. The contents of alloying elements in Zr-4 samples are listed in Table 1.

Then, zirconium sheet samples with a thickness of 1.0 mm were fabricated with the standard processing (Fig.1) including β-forging at 1030 °C, β-quenching at 1030 °C, α-hot rolling at 640 °C, and several cold-rolling steps with intermediate α-annealing at 640 °C for 3~5 h. Finally, the sheet samples were annealed for recrystallization.

1.2 Tube sample preparation

After the corrosion property optimization, the composition with the best corrosion resistance was used for tube sample experiment. Two 5 t Zr-4 alloy ingots were prepared with three vacuum self-consumption smelting and the diameter of the samples was 700 mm. Then, the ingots were forged into billets and their diameter was 225 mm. Billets were water quenched immediately after heating at 1093 °C for 90 s. A thermocouple in each billet was used to measure the cooling rate which was located at 3 mm depth inside the sample. The two billets were hot extruded at approximately 650 °C for a very short time, and then annealed at 635 °C for 1 h. After the cold reduction followed by annealing at 635 °C for several times, the TREX tube (Φ63.5 mm×10.92 mm, tube of reduction and extrusion) and final cladding tube (Φ9.5 mm×0.57 mm) were fabricated.

1.3 Corrosion test

Long-term corrosion tests were performed on the sheet samples in steam at 400 °C/10.3 MPa for 300 d and 420 °C/10.3 MPa for 150 d in static autoclaves. The TREX tube samples were tested in steam at 400 °C/10.3 MPa for 300 d, 420 °C/10.3 MPa for 126 d, and 500 °C/10.3 MPa for 8, 16, and 32 h. The hydrogen content of the TREX tube samples corroded at 400 °C for 300 d and 420 °C for 126 d was analyzed by the following process. Firstly, the physical stain was removed from the surface of corroded samples with the acetone. And then, part of the sample was put into the equipment together with the flux for melting to release the hydrogen completely. Finally, the hydrogen content released from the sample in step 2 was accurately measured by RH600 hydrogen meter. The nickel content in the sheet and tube samples was determined by ICP-OES spectrometer after the samples were dissolved in the mixture of HF and HNO_3 acid. Five parallel samples were tested under each condition. And the result deviation was ±5 μL/L.

Table 1 Chemical composition of three Zr-4 sheet samples and ASTM standard (wt%)

No.	Sn	Fe+Cr	C	Si	Ni
1#	1.30	0.31	0.0035	0.0101	0.0015
2#	1.31	0.30	0.0034	0.0100	0.0035
3#	1.30	0.31	0.0035	0.0102	0.0050
ASTM-R60804	1.20~1.70	0.28~0.37	＜0.020	＜0.012	＜0.007

1.4 Microstructure analysis

The morphology of oxide formed on the outer surface of Zr-4 tubes was characterized by a Leica DM2500M metallographic microscope. The size, quantity, and distribution of the second phase particles in the sheet samples were analyzed by a NOVA Nano450 scanning electron microscope. The polarization on the interface between the matrix and second phase particles was analyzed by the high resolution transmission electron microscope (HRTEM), the energy dispersive spectroscopy (EDS), and the selected area electron diffraction (SAED).

2 Results and Discussion

2.1 Effect of nickel content on the corrosion properties of sheet samples

The mass gain as a function of Ni content for the sheet samples in steam at 400 and 420 °C is shown in Fig.2a. The Ni content in sponge zirconium is usually lower than 0.0015wt%. It shows that the mass gain at both temperatures decreases with the increase in the Ni content. In particular, the mass gain of the sample with Ni content of 0.0035wt% is 119.05 mg/dm^2 and that of the sample with Ni content of 0.0050wt% is 102.45 mg/dm^2 under 400 °C, 300 d. Meanwhile, the mass gain of the sample without Ni addition is 140.43 mg/dm^2. The mass gain measured under the condition of 420 °C, 150 d is almost the same as that under the condition of 400 °C, 300 d, which indicates that a higher temperature can accelerate corrosion rate. In general, the mass gain data show that a small amount of Ni addition in Zr-4

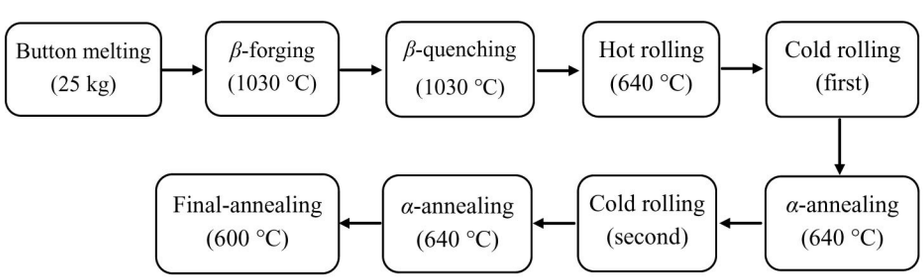

Fig.1 Processing sequence of zirconium sheet samples

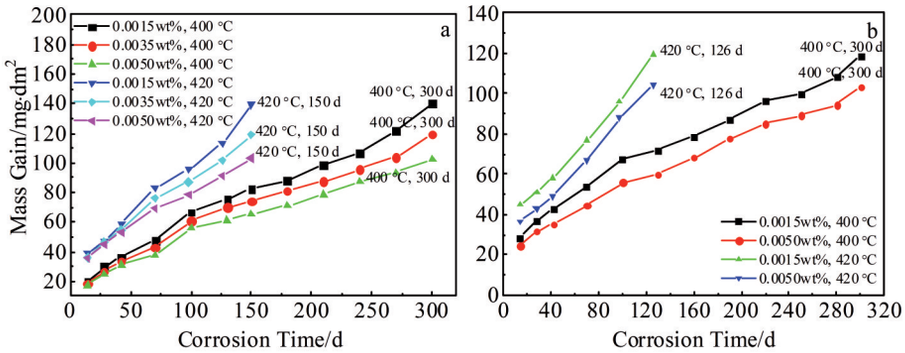

Fig.2 Mass gain as a function of Ni content at 400 and 420 °C: (a) sheet samples and (b) tube samples

alloy can improve its uniform corrosion resistance.

The surfaces of the sheet samples with different Ni contents exposed in steam at 400 °C for 300 d and 420 °C for 150 d are shown in Fig. 3. On the surfaces of the samples without extra nickel addition, gray spots appear under the two different corrosion conditions (Fig. 3a and 3d). However, when extra trace nickel is added to the samples, the corrosion spots almost cannot be found on the surfaces of those samples. This result agrees with mass gain tests: mass gain is slower for the samples with extra nickel addition.

2.2 Effect of nickel content on corrosion properties of the TREX samples

Based on the result of corrosion tests, the composition design of the sheet sample with the best corrosion property was used to prepare a TREX sample (Φ63.5 mm×10.92 mm). The mass gain as a function of Ni content at 400 and 420 °C is shown in Fig. 2b. Compared with the sample without extra trace nickel, the mass gain at 400 °C for 300 d is reduced by about 15 mg/dm^2 for the sample with extra trace nickel. A similar phenomenon can be found in the corrosion tests at 420 °C. In general, the corrosion properties of Zr-4 alloy can be improved by adding a small amount of nickel alloying element.

In order to investigate the effect of extra trace nickel on the nodular corrosion performance of TREX tubes, the samples were corroded in the steam under the condition of 500 °C and 10.3 MPa for 8, 16, and 32 h. The surface morphologies of the samples are shown in Fig. 4. It shows that the inner and outer surfaces of the samples with extra nickel addition are still black and shiny after 32 h. However, a small amount of nodular spots can be found on the inner surface of the sample without extra Ni after 8 h. With the increase in corrosion time, the nodular spots increases both in number and in size.

The mass gain of tube with extra nickel was compared with that of the one without extra nickel addition and the results are shown in Fig. 5. It shows that the extra nickel can improve

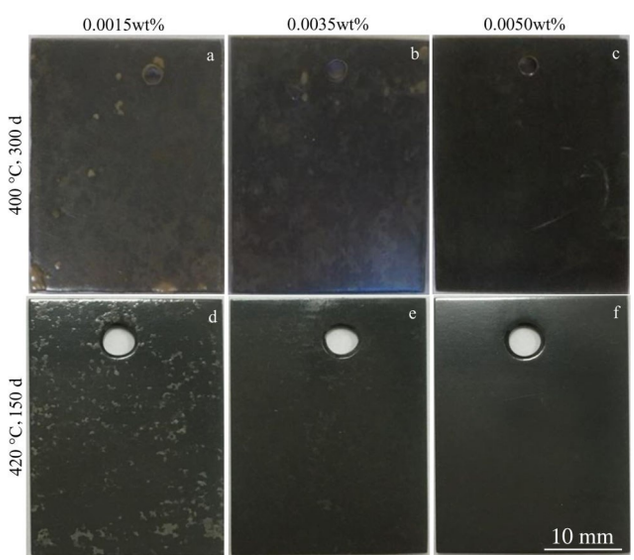

Fig.3 Surface morphologies of the sheet samples with different Ni contents at 400 °C for 300 d (a~c) and 420 °C for 150 d (d~f): (a, d) 0.0015wt%, (b, e) 0.0035wt%, and (c, f) 0.0050wt%

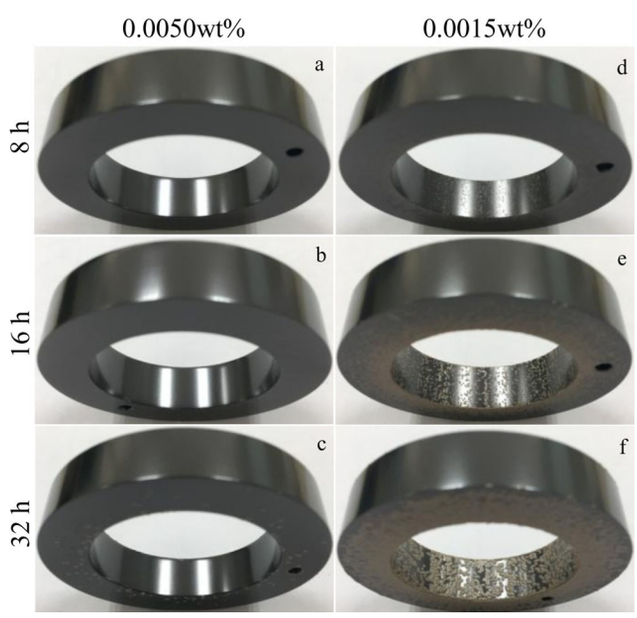

Fig.4 Surface morphologies of TREX samples with different Ni contents at 500 °C for different time: (a) 0.0050wt%, 8 h; (b) 0.0050wt%, 16 h; (c) 0.0050wt%, 32 h; (d) 0.0015wt%, 8 h; (e) 0.0015wt%, 16 h; (f) 0.0015wt%, 32 h

nodular corrosion resistance of TREX tubes.

2.3 Effect of nickel content content on hydrogen content of TREX tube samples

Hydrogen content is an important issue for the zirconium alloy. The effect of trace nickel on the hydrogen content of TREX tube samples was evaluated and the results are shown in Fig. 6. According to the results of the corrosion tests at 400 °C for 300 d, it is found that the hydrogen content is not sensitive to the nickel content. At 420 °C, similar results were observed. Although the hydrogen content is not sensitive to the nickel content, the adsorption rate at 420 °C is higher than that at 400 °C due to the temperature effects. In addition, the final cladding tubes tested at 400 °C for 300 d were also compared with the TREX, and it can be seen that the hydrogen content is slightly lower than that of the TREX at the same nickel content, which may be due to the geometry.

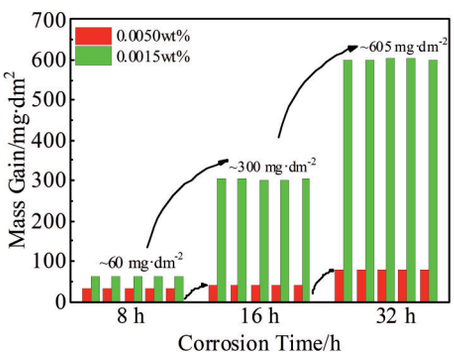

Fig.5 Mass gain of TREX tube as a function of Ni content at 500 °C for 8 h, 16 h, and 32 h

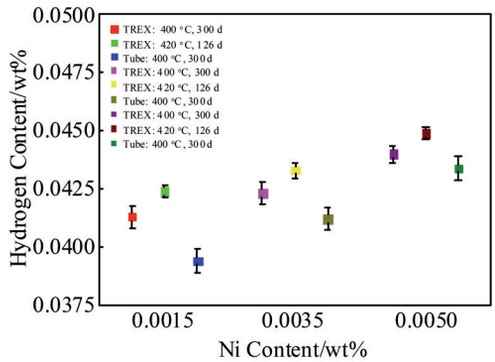

Fig. 6 Hydrogen content as a function of Ni content at 400 °C for 300 d and at 420 °C for 126 d

Therefore, in general trace nickel addition does not change the hydrogen content although it can improve the uniform corrosion resistance.

2.4 Microstructure analysis

Another issue that may affect the corrosion properties is the distribution of second phase particles on the surface of sheet samples with different nickel contents. HRSEM was used to study the distribution of the second phase particles on the surface of sheet samples, as shown in Fig.7. The results are as follows. (1) The second phase particles are uniformly distributed in the samples with different nickel contents. (2) The average size of the second phase particles is independent of the nickel content and the diameters of them are 75~78 nm. (3) The area fraction increases with the increase of nickel content from 1.21% to 1.61%. As a result,

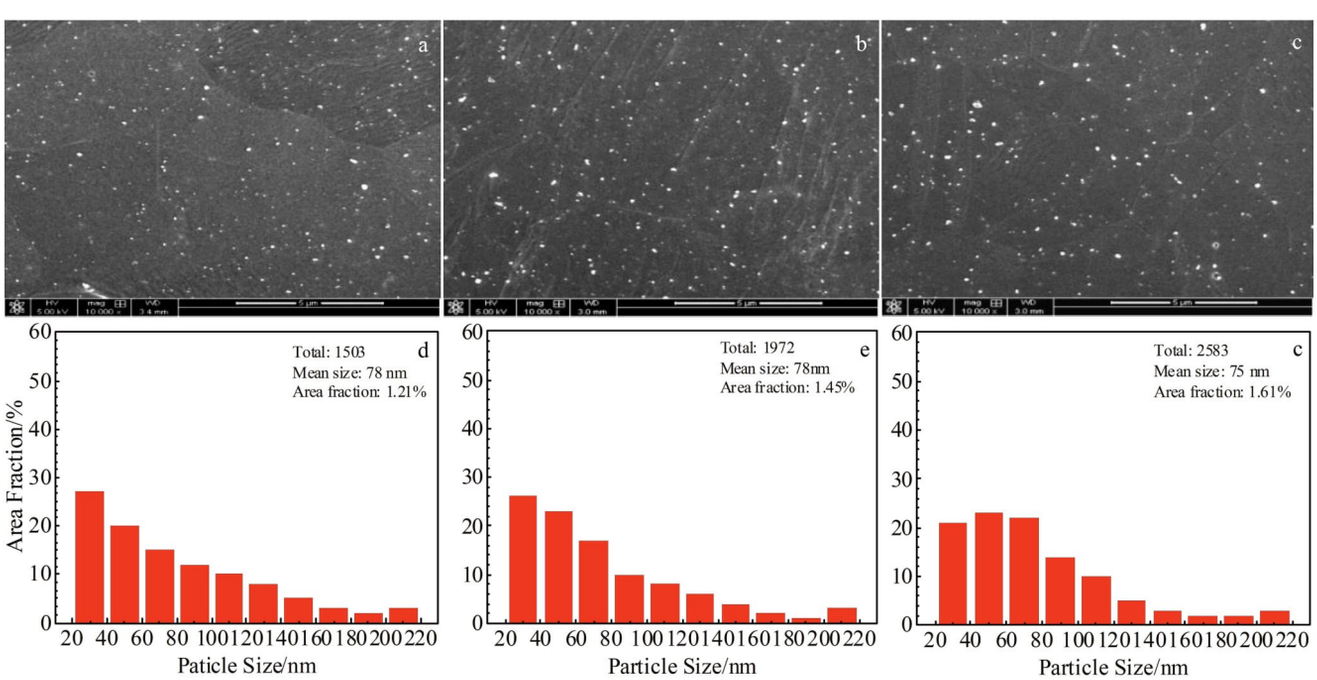

Fig.7 HRSEM images (a~c) and distribution (d~f) of second phase particles in the sheet samples with differetn Ni contents: (a, d) 0.0015wt%, (b, e) 0.0035wt%, and (c, f) 0.0050wt%

the extra trace nickel addition favors the formation of the precipitates.

The composition of second phase particles was analyzed by high angle annular dark field (HAADF) image and EDS mapping. Most of the second phase particles are $Zr(Fe, Cr)_2$, while a small amount of the particles are $Zr_2(Fe,Ni)$, shown by arrows in Fig. 8a. In the sample without extra nickel addition, only $Zr(Fe, Cr)_2$ particles are found. It suggests that if the nickel content is higher than the solubility, the extra nickel added will promote the formation of $Zr_2(Fe, Ni)$ precipitation. In addition, the segregation of Si is found around the second phase particles in the sample with extra nickel (Fig. 8a). This situation does not happen in the sample without extra nickel.

The structure of the Si segregation area was analyzed by HAADF images and SAED and the results are shown in Fig. 9. The arrow 1 in Fig. 9a points to the second phase particles of hcp-$Zr(Fe,Cr)_2$ and arrow 2 points to the Si-enriched area. The results show that the NiSi particles form with tetragonal structure in the Si-enriched area. In addition, NiSi precipitation cannot be found in the samples without extra nickel addition while hcp-$Zr(Fe,Cr)_2$ precipitation indicated by arrow 1 still can be seen in Fig. 10.

2.5 Relationship between microstructure and corrosion properties

It is well known that the corrosion resistance of Zr-4 alloy is closely related to the distribution of second phase particles[29-34]. Particularly, samples with uniformly distributed small second phase particles show good nodular corrosion resistance[35]; while the samples with uniformly distributed large size particles can increase the long-term uniform corrosion performance[36]. Thorvaldsson et al[37] introduced that the uniform corrosion behavior of Zircaloy-4 has been determined in long-term autoclave tests at 400 °C and mo-

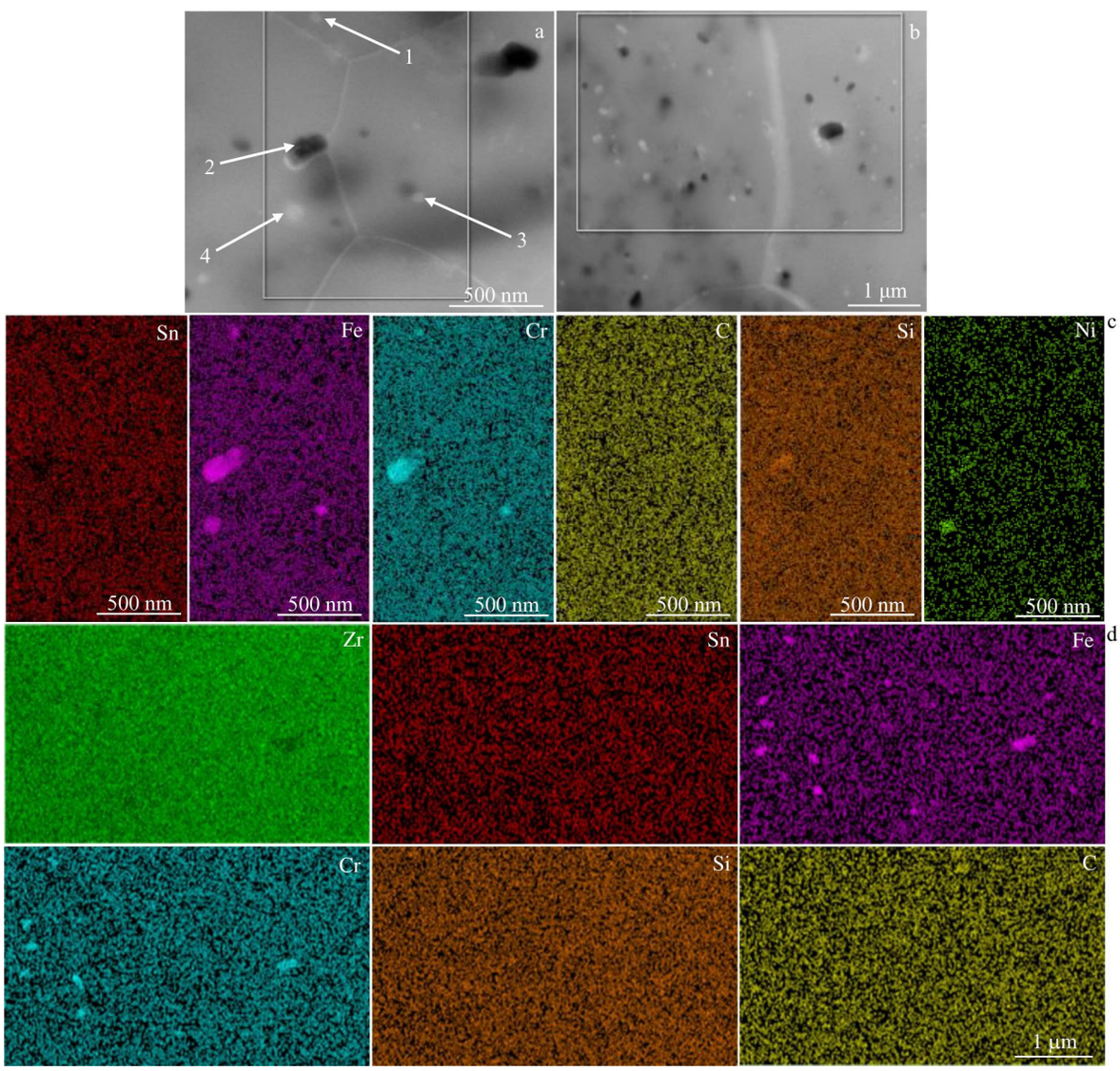

Fig.8 HAADF images (a, b) and corresponding EDS mappings for square area (c, d) of samples with different nickel contents: (a, c) 0.0050wt% and (b, d) 0.0015wt%

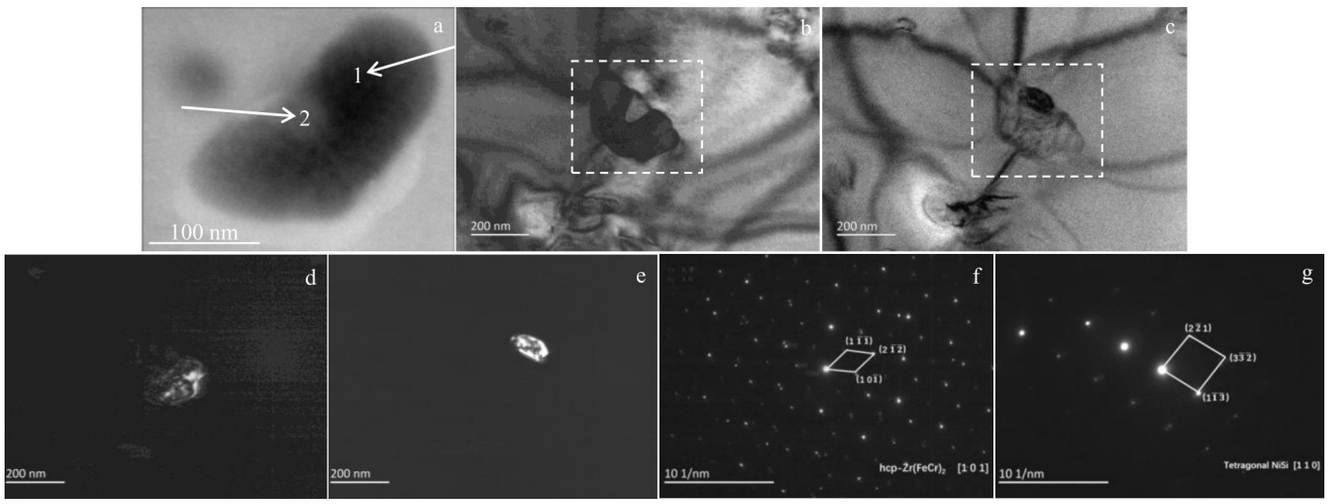

Fig.9 HAADF image (a), TEM bright field images (b, c), TEM dark field images (d, e), and SAED patterns (f, g) of the second phase particles in the sample with extra nickel addition: (b, d, f) hcp-Zr(Fe,Cr)$_2$ marked by arrow 1 in Fig.9a and (c, e, g) Si-enriched area marked by arrow 2 in Fig.9a

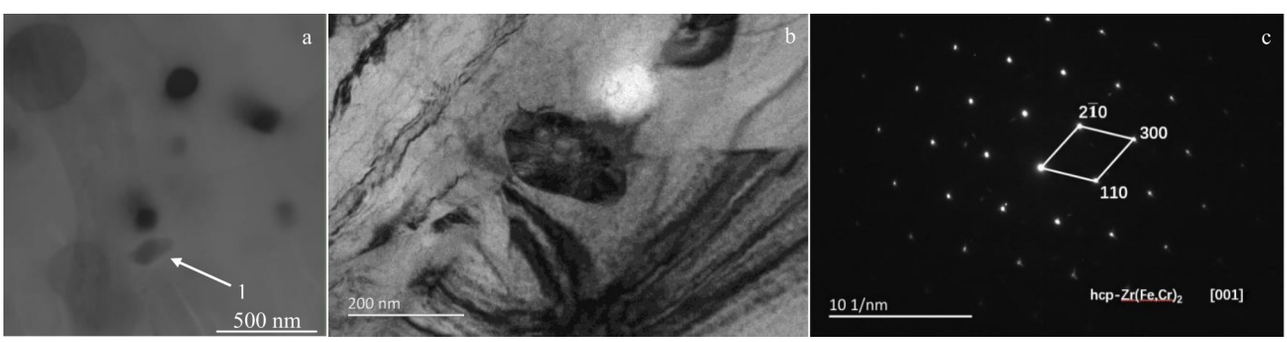

Fig.10 HAADF image of second phase particles (a), and TEM bright field image (b) and SAED pattern (c) of arrow 1 in Zr-4 samples without extra nickel addition

deled using the annealing parameter A concept. The cumulative effect of subsequent heat treatments in the α phase field after β-quenching can be given by $A=\sum_i t_i \exp(Q/RT_i)$, where t_i is annealing time, T_i is the temperature, Q is the activation energy, and R is the gas constant. Alheritiere et al[38] proposed that a combination of fast cooling rate and certain composition can improve the nodular corrosion resistance, while appropriate accumulative annealing A value will result in better uniform corrosion resistance. Anada[39] pointed out that if the A value is insufficient, a large number of fine second phase particles will be distributed on the surfaces of the samples. As a result, as shown Fig. 11a and 11c, oxygen ions may diffuse from the outer oxide-film into the second phase particles and form FeO and Cr_2O_3 which induce local stress and structural deformation. The columnar structure of local ZrO_2 oxide film will be destroyed and begin to transform into fine equiaxed structure. As shown in Fig. 11e and 11g, further evolution will result in macroscopic local "island" spots. Correspondingly, it shows higher corrosion mass gain than the samples with fine equiaxed structure. Since it is difficult to accurately control the annealing parameter A during the processing stage, alloying element optimization can be used to generate well distributed second phase particles which can uniformly protect the zirconium alloy.

According to this research, it can be concluded that there are two positive effects by adding trace Ni to Zr-4 alloy within the ASTM range. On the one hand, the precipitation amount of second phase particles in the sample is significantly increased; on the other hand, from Fig.11b and 11d, it can be seen that the addition of Ni promotes the enrichment of Si around the fine second phase particles in the form of NiSi tetragonal structure. Such two effects will hinder or delay the diffusion process of external O^{2-}, and ensure that the columnar crystal proportion of the ZrO_2 film is predominant with uniform and consistent thickness macroscopically (Fig.11f and 11h), while the equiaxed crystal proportion is less in the whole cycle of corrosion.

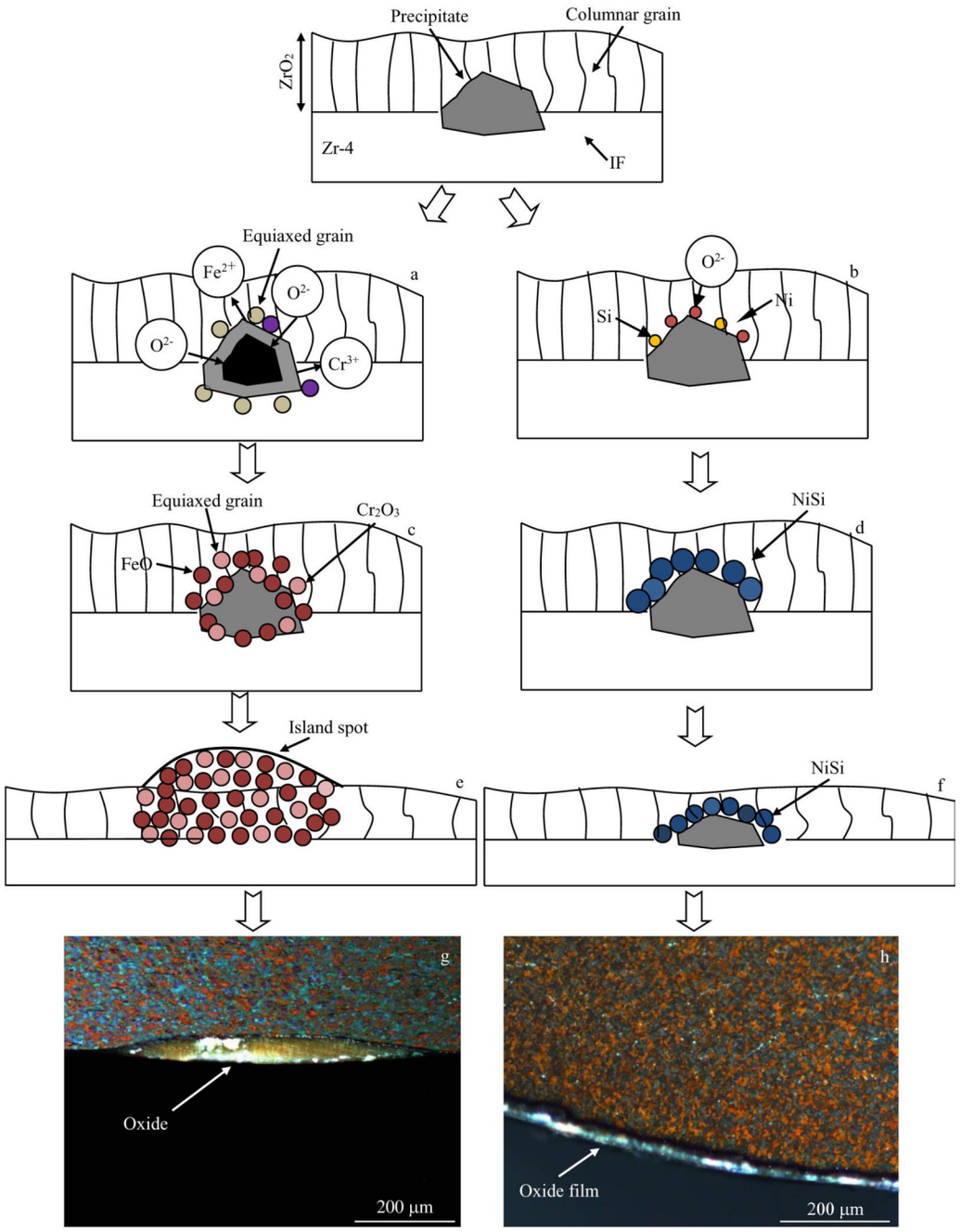

Fig.11 Effect of different Ni contents on the second phase particles: (a, c, e, g) low Ni content and (b, d, f, h) high Ni content

3 Conclusions

1) Extra nickel addition in Zr-4 alloy can significantly improve its corrosion resistance without deteriorating its hydrogen absorption properties. The cladding tube with extra nickel also shows excellent nodular corrosion and long-term uniform corrosion performance.

2) The addition of trace nickel promotes the precipitation of second phase particles in the form of $Zr(Fe, Cr)_2$ and $Zr_2(Fe, Ni)$, and the enrichment of silicon in the form of NiSi around the second phase particles. As a result, it hinders or delays the oxidation process of fine particles and thus improves the corrosion resistance of the Zr-4 alloy.

3) Although a higher value of cumulative annealing parameter A can provide better corrosion properties, the optimized alloy composition can adjust the distribution of the second phase and form a protective layer for the Zr-4 alloy cladding tubes. Particularly, it is easy to obtain more stable corrosion properties in actual industrial production.

References

1 Feng Z H, Li D, Dong H C *et al. Materials Characterization*[J], 2021, 172: 110 873

2 Jailin T, Tardif N, Desquines J. *Materials Characterization*[J], 2020, 161: 110 199

3 Sabol G P, McDonald S G. *Nuclear Science and Engineering*[J], 2017, 63(1): 83
4 Abdel-Aziz Fahmy Waheed, Abdel-Hakim Taha Kandil, Hani M Hamed. *Annals of Nuclear Energy*[J], 2016, 94: 168
5 Zhang Xin, Yao Meiyi, Peng Jianchao *et al. Rare Metal Materials and Engineering*[J], 2017, 46(12): 3910 (in Chinese)
6 Zhang Jinlong, Tu Liming, Xie Xingfei *et al. Journal of Chinese Society for Corrosion and Protection*[J], 2014, 34(2): 171 (in Chinese)
7 Li Shilu, Yao Meiyi, Zhang Xin *et al. Acta Metallurgica Sinica*[J], 2011, 47(2): 163 (in Chinese)
8 Yao Meiyi, Li Shilu, Zhang Xin *et al. Acta Metallurgica Sinica*[J], 2011, 47(7): 865 (in Chinese)
9 Hou Keke, Huang Jiao, Yao Meiyi *et al. Rare Metal Materials and Engineering*[J], 2019, 48(5): 1440
10 Gou S Q, Zhou B X, Chen C M *et al. Corrosion Science*[J], 2015, 92(3): 237
11 Chai Linjiang, Chen Baofeng, Zhou Zhiming *et al. Materials Characterization*[J], 2015, 104: 61
12 Yao M Y, Zhou B X, Li Q *et al. Journal of Nuclear Materials*[J], 2008, 374(1): 197
13 Ni Jia, Zha Yicheng, Wang Lian *et al. Nuclear Materials and Energy*[J], 2018, 17: 158
14 Sawabe T, Sonoda T, Furuya M *et al. Journal of Nuclear Materials*[J], 2015, 466: 658
15 Wanklyn J N, Britton C F, Silvester D R *et al. Journal of the Electrochemical Society*[J], 2019, 110(8): 856
16 Wu Yue, Chen Bin, Lin Xiaodong *et al. Rare Metal Materials and Engineering*[J], 2021, 50(12): 4437 (in Chinese)
17 Maussner G, Steinberg E, Tenckhoff E. *7th International Symposium on Zirconium in the Nuclear Industry*[C]. Philadelphia: ASTM, 1987: 307
18 Wen Huiming, Li Fan, Ding Yuhang. *Nonferrous Metals Processing*[J], 2021, 50(2): 32 (in Chinese)
19 Sayers J, Lozano-Perez S, Ortner S R. *Corrosion Science*[J], 2019(9), 158: 108 072
20 Than Y R, Grimes R W, Bell B D C *et al. Journal of Nuclear Materials*[J], 2020, 530(3): 151 956
21 Ensor B, Lucente A M, Frederick M J *et al. Journal of Nuclear Materials*[J], 2017, 496(12): 301
22 Kiyoko Takeda, Makoto Harada, Yoshiaki Ishii *et al. Journal of Nuclear Science and Technology*[J], 2006, 43(9): 984
23 Birch Ruth, Wang Siyang, Tong Vivian *et al. Journal of Nuclear Materials*[J], 2019, 513: 221
24 Liu Wenqin, Zhou Bangxin, Li Qiang *et al. Rare Metals*[J], 2004, 3: 286
25 Ogata K. *8th International Symposium on Zirconium in the Nuclear Industry* [C]. Philadelphia: ASTM, 1989: 346
26 Kashif I Choudhry, Igor M Svishchev. *Material and Corrosion*[J], 2020, 71(2): 242
27 Mouton Isabelle, Chang Yanhong, Chakraborty Poulami *et al. Journal of Materialia*[J], 2021, 15: 101 006
28 Chu Linhua, Yuan Gaihuan, Yao Meiyi *et al. Rare Metal Materials and Engineering*[J], 2020, 49(10): 3338
29 Hu Jing, Garner Alistair, Ni Na *et al. Micron: The International Research and Review Journal for Microscopy*[J], 2015, 69: 35
30 Gou Shaoqiu, Zhou Bangxin, Chen Chuanming *et al. Corrosion Science*[J], 2015, 92: 237
31 Godlewski J. *10th International Symposium on Zirconium in the Nuclear Industry*[C]. Philadelphia: ASTM, 1994: 663
32 Kiyoko Takeda, Hiroyuki Anada, Haruhiko Kajimura. *Journal of the Japan Institute of Metals and Materials*[J], 1996, 60(9): 848
33 Lee Cheol Min, Kim Gyeonghun, Sohn Dong-Seong *et al. Journal of Nuclear Materials*[J], 2019,12, 526: 151 749
34 Zhang Yingdong, Yuan Fusen, Han Fuzhou *et al. Journal of Materials Science & Technology*[J], 2020, 47(12): 68
35 Liao Jingjing, Yang Zhongbo, Qiu Shaoyu *et al. Acta Metallurgica Sinicia*[J], 2019, 32(8): 981
36 Yang Zhongbo, Cheng Zhuqing, Qiu Jun *et al. Rare Metal Materials and Engineering*[J], 2018, 47(3): 794
37 Thorvaldsson T, Andersson T, Wilson A *et al. 8th International Symposium on Zirconium in the Nuclear Industry*[C]. Philadelphia: ASTM, 1989: 128
38 Alheritiere E, Charquet D. *7th International Symposium on Zirconium in the Nuclear Industry*[C]. Philadelphia: ASTM, 1987: 284
39 Anada H, Herb B J, Nomoto K *et al. 11th International Symposium on Zirconium in the Nuclear Industry*[C]. Garmisch-Partenkirchen: ASTM, 1996: 74

微量镍元素添加对Zr-4合金微观结构、耐腐蚀性能及吸氢行为的影响

储林华[1]，张书彦[1]，袁改焕[2]，吴桂毅[1]

(1. 东莞材料基因高等理工研究院，广东 东莞 523808)

(2. 国核宝钛锆业股份公司，陕西 宝鸡 721013)

摘　要：将微量镍元素合金化添加到Zr-4合金中，制备了合金板材试样。利用板材试样研究了微量镍元素的添加对Zr-4合金微观结构、耐腐蚀及吸氢性能的影响。结果表明，将镍元素含量由海绵锆原料中的0.001%（质量分数）以下添加至0.005%，可大幅提升其400 ℃蒸汽下耐腐蚀性能，同时对吸氢性能没有明显影响。微量镍元素的添加，不仅使$Zr(Fe, Ni)_2$结构的第二相粒子明显增加，同时还促进了硅在第二相粒子周围的偏聚，这可以阻止或延缓细小第二相粒子被氧化的进程。进一步采用相同合金成分制备的锆管（Φ63.5 mm×10.92 mm），也呈现出了优异的耐疖状腐蚀和耐均匀腐蚀性能。

关键词：镍元素；Zr-4；微观结构；耐腐蚀性能；吸氢；偏聚；氧化

作者简介：储林华，男，1984年生，博士，高级工程师，东莞材料基因高等理工研究院，广东 东莞 523808，E-mail：linhua.chu@ceamat.com